

# Simulation of an Inverse Schlieren Image Acquisition System for Inspecting Transparent Objects

Johannes Meyer<sup>a</sup>, Robin Gruna<sup>b</sup>, Thomas Längle<sup>b</sup> and Jürgen Beyerer<sup>b</sup>

<sup>a</sup> Karlsruhe Institute of Technology (KIT), Adenauerring 4, Karlsruhe, Germany;

<sup>b</sup> Fraunhofer Institute of Optronics, System Technologies and Image Exploitation, Fraunhoferstraße 1, Karlsruhe, Germany

## Abstract

This paper describes a novel approach for inspecting transparent objects. Since the underlying optical setup is based on a schlieren setup, any defect can be detected that leads to the deflection or extinction of incident light rays. By capturing a light field image of a defect-free transparent object and by illuminating objects under test with that very light field, the proposed inspection system can visualize defects by acquiring a single inspection image only. In order to evaluate the presented approach, a physically based rendering framework is used. It is extended by models and implementations of the necessary emitter and sensor plugins. Simulation experiments with virtual scenes that consist of a double-convex lens affected by different types of defects are the basis for a qualitative evaluation of the proposed method. The results show that a single image acquired with the described method is sufficient to test transparent objects for defects that cause the deflection or extinction of rays, e.g., enclosed absorbing or scattering impurities, shape anomalies, differences of the index of refraction and 3D-misalignments.

## 1 Introduction

Transparent objects play an important role in many industrial fields. They are used as lenses in optical systems, as windshields for automobiles or to guide laser beams in eye surgery. Obviously, such applications make high demands on the quality of the employed transparent components: they have to be free from absorbing or scattering impurities and their 3D-surface shape has to be accurately manufactured [11]. There exist machine vision methods for reliably finding absorbing particles in transparent materials. However, detecting shape anomalies of transparent objects is more difficult and still poses challenging problems since elaborated methods like laser triangulation or deflectometry require opaque, respectively, specular surfaces. Also differences in the index of refraction are hard to detect. Schlieren setups (see Sec. 1.1) have been successfully employed to perform deflectometric measurements of the surfaces of transparent objects. Yet, these methods require multiple images to reconstruct the whole surface, what renders them unusable for performing visual inspection in a production site (see Sec. 2). In summary, a method allowing a fast inspection of the deflection characteristics of transparent objects still has to be found. In Sec. 3, this contribution introduces a novel way of inversely using a schlieren setup for inspecting transparent objects. Although some of the required light field components are already available, they still lack the accuracy necessary for automated visual inspection applications. This is why no prototype has been built yet and no real experiments have been conducted. Instead, an adequately constructed model

(see Sec. 4.2) and different simulations using computer graphics state the method's capabilities (see Sec. 5). Further considerations cope with the practical feasibility of the method (see Sec. 6).

### 1.1 Conventional schlieren setup

The conventional schlieren setup (see Fig. 1) has originally been introduced in order to visualize local differences of the index of refraction inside transparent media [2, 15]. A point light source is placed in the focal point of a lens  $L_1$  to illuminate the test object with a collimated light beam. Any change of the index of refraction not oriented parallel to the collimated light beam will result in a local deflection of incident rays. A second lens  $L_2$  placed behind the test object focuses the light beam. If a light ray is deflected by an angle  $\alpha$  inside the measurement range, it will be subject to a certain translation normal to the optical axis at the focal plane of  $L_2$ . The translation is proportional to the deflection angle  $\alpha$ . A so-called schlieren stop that is placed in the focal plane of  $L_2$  acts like a filter selecting certain deflection angles. For example in the setup shown in Fig. 1, only rays deflected upwards (red ray in Fig. 1) inside the measurement range are able to pass the schlieren stop and to contribute to the image formed on the sensor. Acquiring images for different configurations of the schlieren stop allows to successively capture the spatial distribution of deflection angles inside the measurement range.

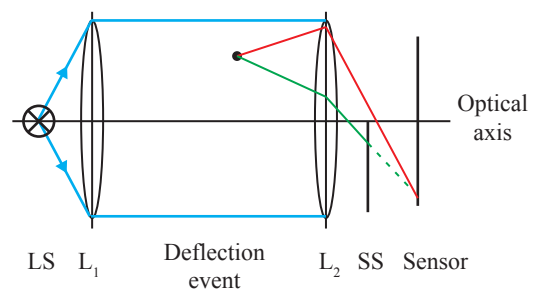


**Figure 1.** Conventional schlieren setup: The lens  $L_1$  collimates the light of the point light source LS. The second lens  $L_2$  collects the parallel beam bundle. Any deflection event occurring between  $L_1$  and  $L_2$  results in rays that miss the focal point of  $L_2$ . Depending on the direction and amount of deflection, the respective rays pass the schlieren stop SS (red ray) or get blocked (green ray).

## 2 Related work

Schlieren setups are used in many fields for the inspection of optical deflection events. With respect to the study of transparent objects there are mainly two relevant previous contributions:

Wetzstein et al. introduce the term *light field background oriented schlieren photography* [21]. They utilize a specially manufactured background illumination that spectrally encodes the direction and the spatial location of the emitted light rays. This background illumination is observed with a camera through a transparent object. The observed colors allow to infer information about the refractive effects taking place on or inside the transparent object. However, they provide no quantitative results. In order to use their proposed method for the visual inspection of a transparent test object, further processing steps would be required in order to perform a complete reconstruction.

Sudhakar et al. try to capture the so-called deflection map of transparent objects [16]. This map spatially resolves the deflection rays undergo when exiting the investigated object at the respective surface location. They employ a schlieren deflectometer capable of illuminating the test object with collimated light beams that are tilted by an adjustable degree with respect to the optical axis. For this purpose they employ a spatial light modulator (SLM) that acts like a binary mask and allows to realize arbitrary patterns of point light sources. This ensemble of point lights is placed in the focal plane of a lens and so yields the mentioned collimated light beams. They use a telecentric camera system to observe the rays deflected by the transparent test object. By this means, they only image such rays that are turned parallel to the optical axis by the deflections occurring inside the test object. They make use of a compressive sensing approach to successively capture the whole deflection map of the inspected object. The acquired information could be used to reconstruct the object and to test it for defects. However, their proposed method requires multiple images in order to obtain all necessary information. Therefore, the method is not suitable for inspecting transparent objects in a production site where the inspection time is a crucial system parameter.

Recently, some novel inspection methods based on inverse illumination approaches have been proposed in the literature. Techniques like inverse fringe projection [3, 14], inverse patterns for deflectometric inspection [18] and comparative digital holography [1, 12] are able to directly highlight differences in the shape of two objects. Defect detection by comparing the actual state of a test object with the desired nominal state of a defect-free reference object is a standard task in industrial inspection. In the case of fringe projection and deflectometry, the shape information of a preceding measurement is used to compute an inverse structured light pattern of the reference object which is then used to evaluate a test object. If the reference object and the test object are identical, a predefined undistorted pattern is obtained. Otherwise, shape differences are directly highlighted by local geometric distortions in the projected pattern. In the case of holography techniques for object comparison, the coherent optical wave field of the reference object is obtained by digital holography. By illuminating the test object with the coherent mask of the reference object, differences in the shape between the two objects are directly visible in the inspection image. Another inverse illumination technique is proposed in [6], which is motivated by light transport inversion in a projector-camera-system. This technique is able to directly highlight shape and reflectance differences in the inspection image with high contrast-to-noise ratio. All the described inspection techniques adapt the illuminating light field to the desired nominal state of the inspection task. Hence, the captured inspec-

tion images directly highlight differences from the nominal state and therefore reduce the effort of defect detection through digital image processing or signal processing. This means that feature extraction for defect detection partly takes place in the optical domain, i.e., during image formation.

### 3 Optical setup

The method presented in this contribution is a two-step approach that requires a completely intact instance of the type of object that is to be inspected.

At first, the intact object instance is illuminated with a collimated light beam. The difference between the object's index of refraction and that of the surrounding medium results in a deflection of the incident rays out of their parallel orientation. A light field sensor placed at a certain distance  $\Delta$  from the object captures the light field  $\mathcal{L}$  consisting of the deflected light rays (see Fig. 2). For first considerations, this sensor is not supposed to represent a physically existing equivalent.

The observed light field  $\mathcal{L}$  now allows to test another object of the same type for defects by means of the following approach. A light field emitter emits the light field  $\mathcal{L}$ . If that emitter is placed exactly at a distance  $\Delta$  from a defect-free test object, this object will transform any incident light rays into rays running parallel to the optical axis. Conversely, any difference of the investigated object to the intact object instance will result in rays that are either blocked or that do not run parallel to the optical axis. A telecentric camera system focused on the test object produces an image where bright pixels represent intact object parts. Rays that passed a defect and therefore do not run parallel to the optical axis get blocked by the telecentric stop and result in dark regions in the captured image. Figure 3 shows an example optical path for both defect-free and defective object parts. Since the test object is focused by the camera, dark image structures allow to infer the defective object parts.

The proposed setup is capable of inspecting the whole object volume by acquiring a single image only. As no tomographic methods are applied, there is no need to rotate the test object. The inverse schlieren method visualizes any kind of defect that results in changed optical paths of the incident light rays with respect to those passing the intact reference object. Example defects that can be visualized by the proposed approach are:

- enclosed contaminants (e.g., opaque particles, air bubbles, cracks),
- defects affecting the 3D-structure,
- inhomogeneities of the index of refraction and
- misalignments with respect to the 3D-position.

### 4 Simulation environment

The physically based rendering framework Mitsuba [8] allows to simulate the proposed approach. The following two sections give details concerning the framework and the introduced plugins respectively.

#### 4.1 Rendering framework

Figure 4 shows a sketch of the basic framework components. Every simulation using this framework consists of a sensor, at least one light source and one or more shapes (e.g., spheres, rectangles or triangle meshes) that can be combined to represent arbi-



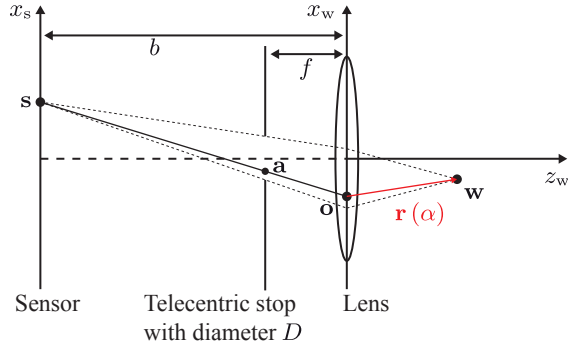


**Figure 5.** Optical concept of the introduced telecentric camera plugin: The ray of sight  $\mathbf{r}(\alpha)$  corresponding to the sensor position  $\mathbf{s}$  and the aperture position  $\mathbf{a}$  is calculated using the thin lens formula and the intercept theorem. The image plane distance  $b$  and the lens' focal length  $f$  are the optical parameters of the camera system.

visualizes the basic layout of the light field sensor. The spatial elements convey the spatial information of the light field and the underlying pixels—the so-called angular elements—convey the angular information about rays passing through the respective spatial element. The parameters fully describing the light field sensor are the pixel size, the number of pixels in  $x$ - and  $y$ -direction and the angular resolution, i.e., the number of angular elements inside a spatial element.

In order to determine the ray of sight  $\mathbf{r}(\alpha) = \mathbf{o} + \alpha \cdot \mathbf{d}$  for a pixel sample  $\mathbf{p} = (p_x, p_y)^T$ , the following steps have to be performed: Since the spatial elements encode the light field's spatial component,  $\mathbf{o}$  is the center of the spatial element corresponding to  $\mathbf{p}$ . The relative position of  $\mathbf{p}$  inside its spatial element encodes the angle of the ray of sight with respect to the sensor plane. In order to avoid the introduction of further parameters, the direction  $\mathbf{d}$  of  $\mathbf{r}(\alpha)$  is defined as follows: The pixel alignment inside a spatial element is projected onto a hemisphere with radius 1 located beneath the sensor plane (see Fig. 7). The vector originating at the position on the hemisphere of the projected point and going through  $\mathbf{o}$  denotes the direction  $\mathbf{d}$ . Any point  $\mathbf{p}$  missing the hemisphere, i.e., for which  $\sqrt{p_x^2 + p_y^2} \geq 1$  is assigned the pixel value 0. Setting the parameters of  $\mathbf{r}(\alpha)$  in this way results in a variable angular resolution inside the spatial elements. Because of the projection onto the hemisphere, the angular resolution decreases for an increasing distance of  $\mathbf{p}$  from the center of the spatial element.

As this model is based on a common two-dimensional sensor, it can be directly realized as a Mitsuba sensor plugin and the captured light field can be stored as a convenient image file. The choice of the angular and spatial resolution is free.

**Light field emitter** The light field emitter plugin is the counterpart of the light field sensor plugin described before. It requires an image file providing the light field to emit and suitable spatial and angular resolution parameters. Besides, the size of the pixels has to be specified.

For any query from the renderer consisting of a position  $\mathbf{q}$  on the emitter and a direction  $\mathbf{d}$  of the incident ray, the corresponding radiance has to be read from the image file. As for the light

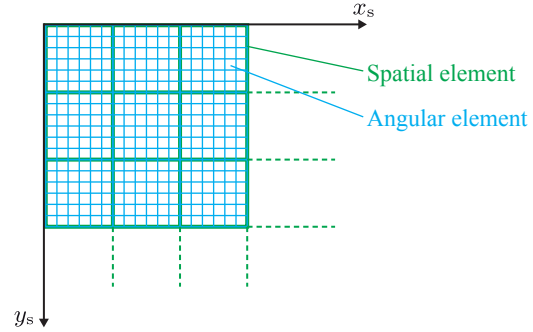


**Figure 6.** Layout of the introduced light field sensor plugin showing the concept of spatial elements and angular elements.

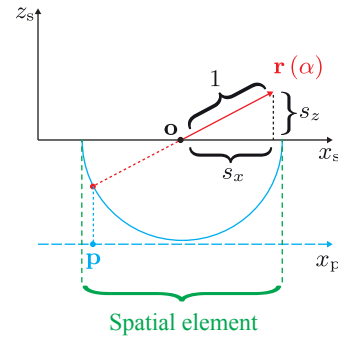


**Figure 7.** Computation of the ray of sight inside a spatial element of the introduced light field sensor: The figure shows a projection onto the  $(x_s, z_s)$ -plane. The sensor sample  $\mathbf{p}$  is projected onto a hemisphere with radius 1 located under the sensor plane. The projected point determines the direction of the ray of sight  $\mathbf{r}(\alpha)$  originating from the center  $\mathbf{o}$  of the respective spatial element.

field sensor plugin, the query ray is assumed to hit the center of a macro pixel. The projection of the unit vector  $\frac{\mathbf{d}}{\|\mathbf{d}\|}$  onto the sensor plane yields the pixel position at which the sought-after radiance is stored in the light field image. This is equivalent to determining  $(p_x, p_y)^T$  for given  $\mathbf{r}(\alpha)$  and  $\mathbf{o}$  in Fig. 7.

**Parallel emitter** At every surface point, the parallel emitter plugin emits light inside a definable cone centered around the respective surface normal (see Fig. 8). A shape, the maximum tolerable angle between the surface normal  $\mathbf{n}$  and the query direction  $\mathbf{d}$  and the radiance  $L$  are the only parameters needed.

## 5 Evaluation

Images of virtual scenes rendered using Mitsuba and the novel plugins introduced in the previous section are the foundation for the evaluation of the proposed method. A double-convex lens is the test object. Certain modifications applied to the test object represent instances of different types of defects. Besides the inverse schlieren illumination method, also setups using a common area illumination and the previously introduced parallel emitter plugin are employed to simulate inspection images. All

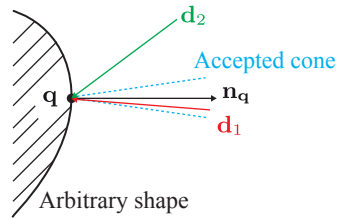


**Figure 8.** Concept of the introduced parallel emitter plugin: Every surface point  $q$  emits radiation inside a cone of definable aperture angle centered around the respective surface normal  $n_q$ . In this example, light is received by query direction  $d_1$  but not by query direction  $d_2$ .

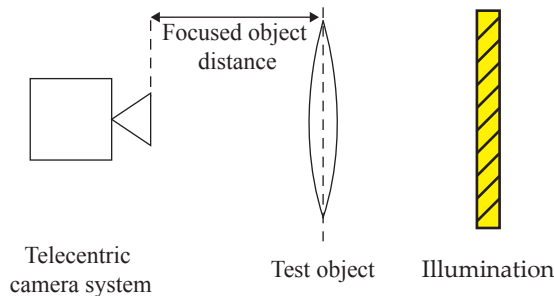


**Figure 9.** Sketch of the experimental setup: The test object—a double-convex lens—is illuminated either by a telecentric (i.e., parallel) illumination, by an area illumination or by the inverse schlieren illumination. The employed telecentric camera system is focused on the test object.

three setups make use of a telecentric camera system. Figure 9 shows a sketch of the virtual experimental setup. The three different simulated images allow to compare the different inspection setups against each other.

### 5.1 Virtual scenes

Every of the created virtual scenes copes with a certain type of material defect which affects the respective test object. The following paragraphs show and discuss the resulting simulated images. Figure 12 shows the simulated images for a defect-free object instance. Since the telecentric camera captures only rays that are approximately parallel to the optical axis, only the center of the test object appears bright in the case of the telecentric illumination. Rays passing the outer regions of the test object are refracted to such an extent that they get blocked by the telecentric stop of the camera. The area illumination emits rays in all directions so that the transparent test object is nearly invisible in the simulated image. The inverse schlieren method also results in an image in which the defect-free test object can barely be seen. Due to the limited resolution of the light field emitter, the test object's margins are slightly visible.

**Enclosed absorbing impurities** This defect type is simulated by two opaque spheres placed inside the test object. One of the spheres is located in the test object's center and the other sphere is placed near the test object's boundary. In practice, defects of this type occur in the form of dust particles or other absorbing contaminants.

Figure 13 shows the simulated inspection images for the dif-

ferent optical setups. Since an absorbing defect blocks any incident ray of light, it should be visible in the inspection image if the respective object region is both illuminated and imaged. This is why the two defects are clearly visible in the images acquired under the inverse schlieren illumination and under the area illumination. The parallel illumination does not reveal the defect located near the test object's boundary. This is because the parallel rays illuminating the test object at the respective position are refracted to such an extent that they are not captured by the telecentric camera.

**Enclosed scattering impurities** In order to model enclosed scattering defects, e.g., enclosed air bubbles, small spheres with an index of refraction different to that of the test object are placed inside the test object. The defects' positions are the same as for the absorbing impurities covered in the previous paragraph.

Figure 14 shows the simulated inspection images for the different optical setups. Scattering defects result in deflections of incident rays into multiple directions. This is why these defects are more clearly visible in the images obtained under the inverse schlieren illumination and under the parallel illumination. These two setups—especially the inverse schlieren method—are sensitive to rays which are deflected away from their actual optical path. As the area illumination emits light rays in multiple directions, scattering defects are barely visible in the captured image.

**Incomplete 3D-shape** Parts of two spheres with different sizes are cut out of the intact double-convex lens by means of constructive solid geometry in order to simulate the respective type of defect [5]. Figure 10 visualizes the test objects of the two virtual scenes. Since the radius of the sphere that is cut out of the lens in test object 1 is rather large, this defect should be clearly visible in all three inspection setups. Conversely, the defect in test object 2 could be hard to detect, as its size is chosen so that its image on the sensor is smaller than the area of a single pixel. In practice, surface scratches or cracks represent instances of this type of defect.

Figure 15 shows the resulting inspection images for test object 1. As expected, the defect is clearly visible in all inspection setups. Only the area illumination and the inverse schlieren approach allow to determine the correct size of the defect. The smaller defect in test object 2 is only barely visible in the inspection image shown in Fig. 11 obtained using the inverse schlieren method. This defect is not captured by the other two inspection setups.

**Differences of the index of refraction** A test object instance with a modified index of refraction represents another type of defect. Such defects are practically relevant for high-precision optical materials that require a homogeneous distribution of the index of refraction [4]. In this virtual scene, the altered index of refraction is 10% greater than for the intact test object.

Figure 16 shows the resulting inspection images of the different optical setups. In the image obtained using the area illumination, the region belonging to the test object appears slightly darker since due to the increased index of refraction not all rays of sight reach the emitter anymore. This is also the case for the parallel illumination setup. Here, the radius of the bright circle located in

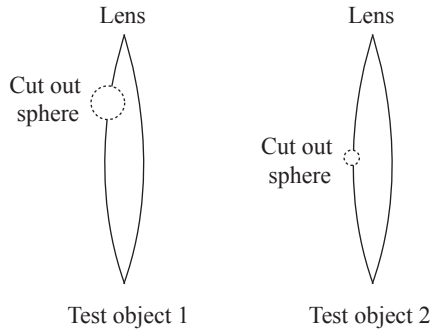


**Figure 10.** Virtual scene for simulating defects resulting in an incomplete 3D-shape: By means of constructive solid geometry, a large and a small sphere is cut out of the test object to simulate defects like cracks or surface scratches.

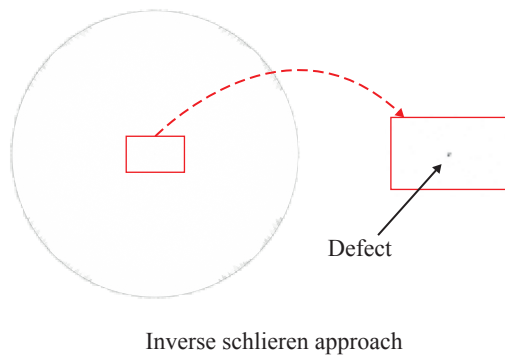


**Figure 11.** Simulated inspection image for test object 2 shown in Fig. 10. The region inside the red rectangle is magnified to make the subpixel size defect visible. The simulated images for the other inspection setups are omitted since they do not visualize the defect.

the center is reduced. That is because rays of sight passing the test object further away from the center are more intensely deflected and thus reach the emitter with an angle of incidence in which no light is emitted.

The altered index of refraction results in different deflection angles of light rays passing all parts of the test object except the object's center where the surface normals are parallel to the propagation direction of the light. Thus, the inspection image obtained using the inverse schlieren method differs to the respective image of an intact object instance at all image positions but the test object's center. In summary, only the inverse schlieren method provides reliable spatial information about the defect.

**3D-misalignment** In this virtual scene the test object is moved out of its intended position along the optical axis. The test object is not moved perpendicular to the optical axis since all three methods would by principle reveal such a misalignment. In practice, such misalignments have to be detected, e.g., in the case of complex and high-precision optical systems where the 3D-positions of the individual components are crucial parameters.

The resulting inspection images are shown in Fig. 17. Apparently, the inspection image obtained with the inverse schlieren method differs mostly with respect to the image of the correctly

positioned test object. Besides a slight blur, the images obtained with the parallel illumination and the area illumination show no indication of a misalignment of the test object. Since the light field emitted by the light field emitter of the inverse schlieren method has been captured for a correctly positioned object, any misalignment of the test object results in a changed deflection characteristic and thus in a different inspection image.

## 6 Discussion

The experiments described in the previous section allow to qualitatively compare the suitability of the studied optical setups with respect to the detection of certain classes of material defects inside transparent objects. Table 1 summarizes the obtained results. In total, these early experiments show that the inverse

**Table 1. Qualitative results of the conducted experiments.** ✓: Defect can be detected; ◦: defect might be detected; ×: defect cannot be detected; <sup>a</sup>: detectability depends on the defect's position; <sup>b</sup>: defects are captured but are hard to detect in the inspection image; <sup>c</sup>: only severe instances of the defect can be detected.

	Parallel illumination	Area illumination	Inverse schlieren
Enclosed absorbing impurity	◦ <sup>a</sup>	✓	✓
Enclosed scattering impurity	◦ <sup>a</sup>	◦ <sup>b</sup>	✓
Incomplete 3D-shape	◦ <sup>ac</sup>	◦ <sup>bc</sup>	✓
Differences of the index of refraction	◦ <sup>a</sup>	◦ <sup>b</sup>	✓
3D-position misalignment	×	×	✓

schlieren method outperforms the other evaluated inspection setups. However, in contrast to the other optical setups, the presented method requires a high resolution light field and a display that is capable of emitting the acquired light field. Such displays are currently being developed for providing consumers with glasses-free 3D-vision [9, 19, 10, 20, 17]. Whether these kinds of displays are suitable for industrial inspection applications still has to be tested.

Another drawback of the presented method is that every individual class of test objects might have a specific optimal distance or even orientation with respect to the light field emitter. Consider the double-convex lens used in the experiments for example. If the light field sensor was placed in the lens' focal point, the sensor would need only a single spatial element with a high angular resolution. Conversely, for increasing distance to the lens, the emitter would have to be large and have a high spatial resolution, i.e., contain many spatial elements with a low angular resolution.

The inverse schlieren method is comparatively sensitive to the position of the test object. Depending on the actual inspection application, this could be an advantage or render the approach inapplicable.

## 7 Conclusion

This paper presents a novel method for visually inspecting transparent objects. The so-called inverse schlieren setup emits an inverse light field that reveals differences of the test object with respect to an intact object instance. By this means, the presented approach is able to detect absorbing or scattering impurities, defects resulting in an incomplete 3D-shape, differences of the index of refraction and a misalignment of the object in 3D-space.

Simulations of the inverse schlieren method using a physically based rendering framework proves the concept and shows that the method is competitive with established optical inspection setups.

However, in order to build a prototype, a suitable way of emitting the light field still has to be found. For this purpose, future work is planned on evaluating different types of light field emitters like 3D-displays using parallax barriers or lenslet arrays and holographic approaches.

## References

- [1] T. Baumbach, W. Osten, C. von Kopylow, and W. Jüptner, "Remote metrology by comparative digital holography," *Applied optics*, vol. 45, no. 5, pp. 925–934, 2006.
- [2] J. Beyerer, F. P. León, and C. Frese, *Machine Vision: Automated Visual Inspection: Theory, Practice and Applications*. Springer Berlin Heidelberg, 2015.
- [3] T. Bothe, W. Li, C. v. Kopylow, and W. Jüptner, "Generation and evaluation of object adapted inverse patterns for projection," *tm-Technisches Messen*, vol. 70, no. 2/2003, pp. 99–103, 2003.
- [4] S. Chatterjee, "Determination of refractive index in-homogeneity of transparent, isotropic optical materials," in *Advances in Optical Science and Engineering*. Springer, 2015, pp. 61–66.
- [5] J. D. Foley, A. Van Dam, S. K. Feiner, J. F. Hughes, and R. L. Phillips, *Introduction to computer graphics*. Addison-Wesley Reading, 1994, vol. 55.
- [6] R. Gruna and J. Beyerer, "On scene-adapted illumination techniques for industrial inspection," in *Instrumentation and Measurement Technology Conference (I2MTC), 2010 IEEE*. IEEE, 2010, pp. 498–503.
- [7] E. Hecht, *Optics*, 4th ed. San Francisco: Pearson, 2013.
- [8] W. Jakob, "Mitsuba renderer," 2010, <http://www.mitsuba-renderer.org>.
- [9] D. Lanman, M. Hirsch, Y. Kim, and R. Raskar, "Content-adaptive parallax barriers: optimizing dual-layer 3d displays using low-rank light field factorization," *ACM Transactions on Graphics (TOG)*, vol. 29, no. 6, p. 163, 2010.
- [10] D. Lanman, G. Wetzstein, M. Hirsch, W. Heidrich, and R. Raskar, "Polarization fields: dynamic light field display using multi-layer lcds," *ACM Transactions on Graphics (TOG)*, vol. 30, no. 6, p. 186, 2011.
- [11] J. Meyer, "Visual inspection of transparent objects – physical basics, existing methods and novel ideas," Karlsruhe Institute of Technology, Tech. Rep. IES-2014-04, 2014.
- [12] W. Osten, T. Baumbach, and W. Jüptner, "Comparative digital holography," *Optics letters*, vol. 27, no. 20, pp. 1764–1766, 2002.
- [13] M. Pharr and G. Humphreys, *Physically based rendering: From theory to implementation*. Morgan Kaufmann, 2004.
- [14] A. Pösch, T. Vynnyk, and E. Reithmeier, "Using inverse fringe projection to speed up the detection of local and global geometry de-

fects on free-form surfaces," in *Image Reconstruction from Incomplete Data VII, SPIE Proceedings on*, 2012, p. 85000B.

- [15] G. S. Settles, *Schlieren and shadowgraph techniques: visualizing phenomena in transparent media*. Springer Science & Business Media, 2012.
- [16] P. Sudhakar, L. Jacques, X. Dubois, P. Antoine, and L. Joannes, "Compressive imaging and characterization of sparse light deflection maps," *arXiv preprint arXiv:1406.6425*, 2014.
- [17] J. Tompkin, S. Heinzele, J. Kautz, and W. Matusik, "Content-adaptive lenticular prints," *ACM Transactions on Graphics (TOG)*, vol. 32, no. 4, p. 133, 2013.
- [18] S. Werling and J. Beyerer, "Inspection of specular surfaces with inverse patterns," *tm-Technisches Messen*, vol. 74, no. 4, pp. 217–223, 2007.
- [19] G. Wetzstein, D. Lanman, W. Heidrich, and R. Raskar, "Layered 3d: tomographic image synthesis for attenuation-based light field and high dynamic range displays," in *ACM Transactions on Graphics (TOG)*, vol. 30, no. 4. ACM, 2011, p. 95.
- [20] G. Wetzstein, D. Lanman, M. Hirsch, and R. Raskar, "Tensor displays: compressive light field synthesis using multilayer displays with directional backlighting," *ACM Trans. Graph.*, vol. 31, no. 4, p. 80, 2012.
- [21] G. Wetzstein, R. Raskar, and W. Heidrich, "Hand-held schlieren photography with light field probes," in *Computational Photography (ICCP), IEEE International Conference on*, 2011, pp. 1–8.

## Author Biography

In 2012 Johannes Meyer received his B.Sc. and in 2014 his M.Sc. in computer science from the Karlsruhe Institute of Technology (KIT) in Germany. Since then he is a PhD student at the Vision and Fusion Laboratory (IES) at the KIT. His research mainly focuses on the automated visual inspection of transparent objects. Johannes Meyer works in close cooperation with the Fraunhofer Institute of Optronics, System Technologies and Image Exploitation (IOSB) in Karlsruhe.

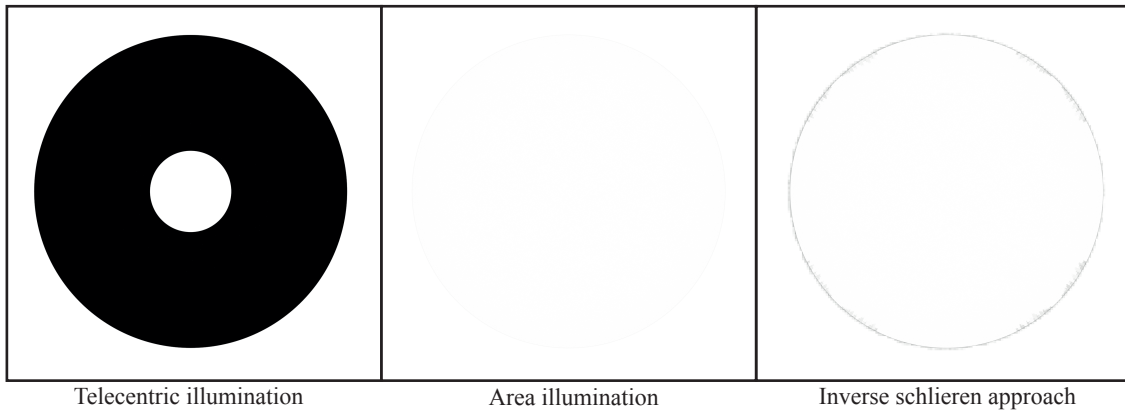


**Figure 12.** Simulated inspection images for an intact, i.e., a defect-free test object.

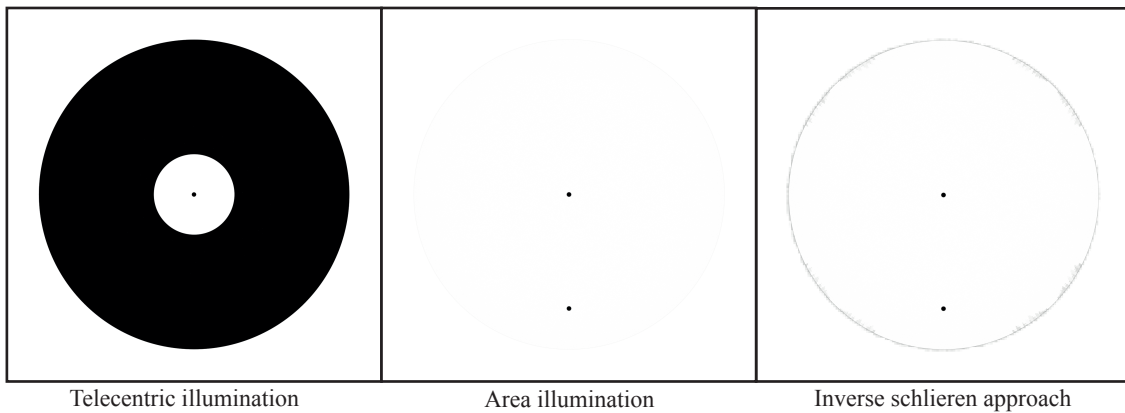


**Figure 13.** Simulated inspection images for a test object containing two absorbing impurities. The defect located in the test object's center is visualized by all three inspection setups with high contrast. The defect located near the boarder of the test object can only be seen in the inspection images obtained using the area illumination and the inverse schlieren approach.

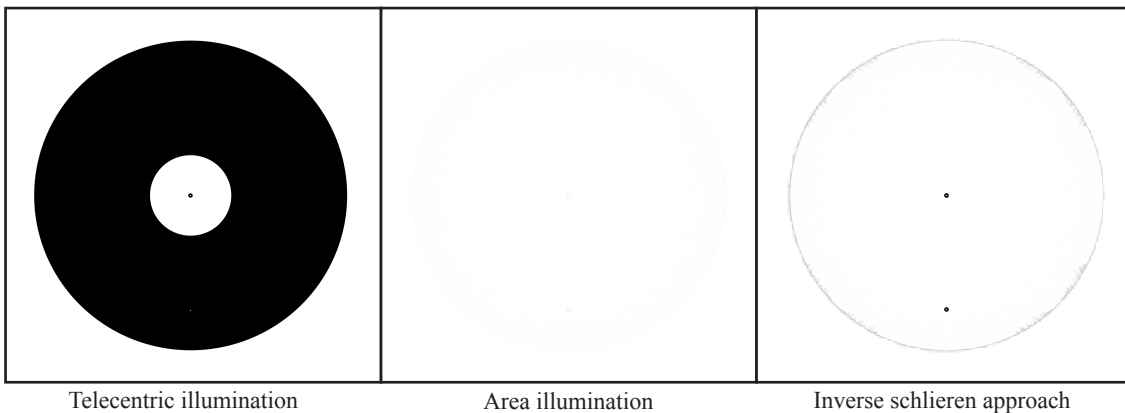


**Figure 14.** Simulated inspection images for a test object containing scattering impurities. The telecentric illumination is capable of revealing the defect in the test object's center with high contrast. The inspection image obtained using the area illumination does not visualize any defect. On the contrary, the inverse schlieren approach shows both defects with high contrast.

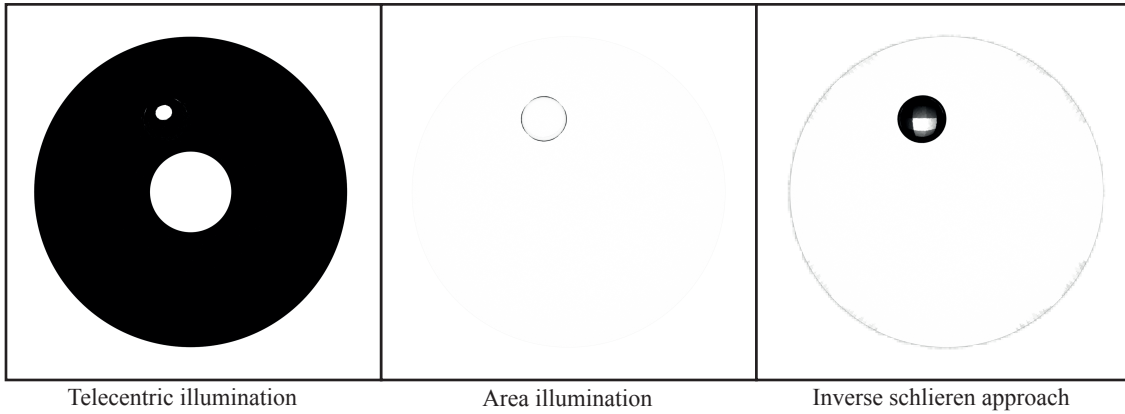


**Figure 15.** Simulated inspection images for a test object with an incomplete 3D-shape (test object 1 shown in Fig. 10). The defect is visible in all three inspection images. However, only the inverse schlieren approach allows to correctly infer the size of the defect.

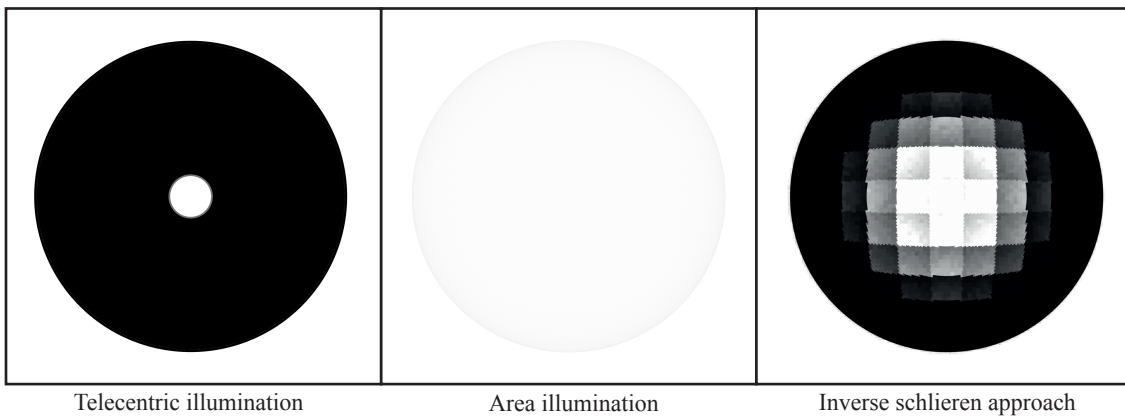


**Figure 16.** Simulated inspection images for a test object whose index of refraction does not match the index of refraction of the reference object. The bright circle in the inspection image obtained using the telecentric illumination has a smaller radius because of the higher index of refraction. The inspection image corresponding to the area illumination is slightly darker since more rays of sight miss the illumination, which allows to infer that the whole volume of the test object is affected by a defect. This also applies to the inspection image resulting from the inverse schlieren approach, where nearly the whole volume of the test object does not direct any light to the camera.

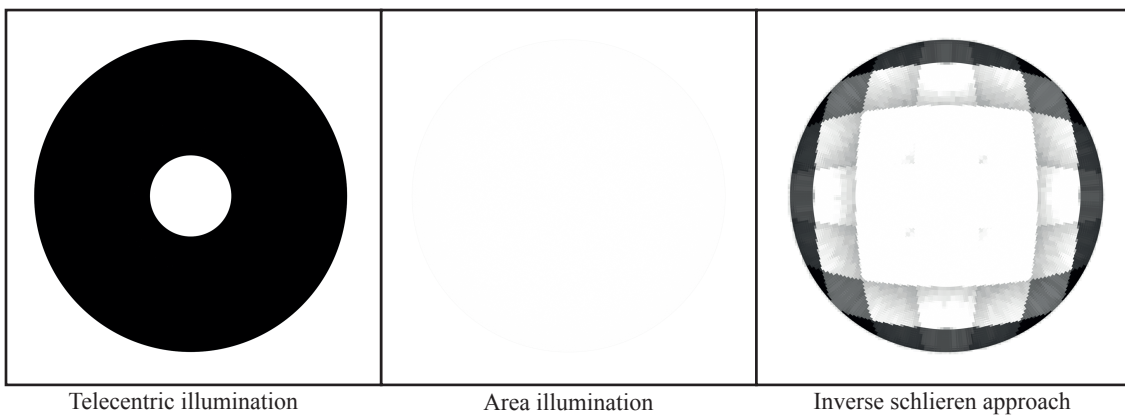


**Figure 17.** Simulated inspection images for a test object that is moved along the optical axis away from its intended position. The misalignment of the test object is only visible in the inspection image obtained using the inverse schlieren approach. In the respective image, the structures visible inside the test object are magnified pixels of the light field emitter.